Dynamic Element Allocation for Optical IRS-Assisted Underwater Wireless Communication System

Rehana Salam[1], Anand Srivastava[1], Vivek Ashok Bohara[1], Ashwin Ashok[2]
[1]Department of Electronics and Communication Engineering, IIIT-Delhi, New Delhi, India, 110020,
[2]Department of Computer Science, Georgia State University, Atlanta, Georgia, 30303, United States
Email: {rehanas, anand, vivek.b}@iiitd.ac.in, aashok@gsu.edu

GLOBECOM 2023 - 2023 IEEE Global Communications Conference | 979-8-3503-1090-0/23/$31.00 ©2023 IEEE | DOI: 10.1109/GLOBECOM54140.2023.10436776

***Abstract*—In view of recent developments in underwater wireless technology and the continuous demand for deep ocean exploration, this study investigates the underwater optical wireless communication system. Underwater wireless optical communication (UWOC) has several benefits over short-distance wireless connectivity due to its significantly higher bandwidth and data rate compared to acoustic communication. This paper presents an analysis of a non-line-of-sight (NLOS) UWOC system configuration using a submerged optical intelligent reflecting surface (OIRS) that is used to support multiple users by allocating different OIRS elements to various users at the receiver end. To increase the average sum rate and preserve user fairness, techniques based on equal mirror assignment (EMA) and distance-based mirror assignment (DMA) are presented. The outcomes are evaluated against conventional orthogonal multiple access (OMA) and non-orthogonal multiple access (NOMA) schemes for underwater communications.**

***Index Terms*—UWOC, NLOS communication, OIRS, Oceanic turbulence, Visible Light Communications (VLC), Exponential and generalized gamma (EGG) distribution.**

I. Introduction

The interest of humans in performing research on underwater operations, such as oceanographic studies, offshore oil exploration, seafloor survey, and monitoring, has increased significantly in the recent years [1]. In order to be effective, underwater wireless communication (UWC) systems need to be reliable as well as support high data rates. In UWC, data is delivered in an unguided aquatic environment via wireless carriers like radio frequency (RF) waves, acoustic waves, and optical waves. Unfortunately, because of the substantial attenuation of RF waves in the oceanic surfaces, its application is restricted. Acoustic waves experience considerably less attenuation, although they are generally hampered by multipath interference, bandwidth restrictions, and significant propagation delays. Optical communication technology is one potential solution for high bandwidth and low latency UWC systems [1]. The UWOC technique outperforms the other two UWC systems in terms of transmission data rate, bandwidth, link delay, and implementation cost. Hence, it can also be employed for real-time data transfer applications [2]. UWOC is also far more secure than RF and acoustic transmission. Consequently, UWOC can effectively collect and analyse data from vast, dangerous, and deep underwater regions without requiring manual human intervention. Despite this, because of the optical signal's significant dispersion and absorption in UWOC, only short-range transmission (less than 200m) is feasible [3]. Mixed dual-hop transmission has been well studied in the literature and is the most popular solution to this issue. Different underwater wireless communication technologies, such as RF, acoustic, and optical, have been comprehensively studied in [1], [3].

According to the literature, there are four different UWOC configurations for data transmission: the point-to-point (P2P) line of sight (LOS) configuration, diffused LOS configuration, retro reflector-based LOS configuration, and NLOS configuration. When direct LOS contact cannot be established between the transmitter and receiver, an NLOS-UWOC setup may be employed. Total internal reflection (TIR) is the underlying theory of NLOS setup. In this configuration, the signal is directed towards the water-air contact, where it is partially refracted and partially reflected at the interfaces of the media having different refractive indices. The reflected signal is transmitted to the receiver (facing the sea surface) [3].

A viable method for overcoming the drawbacks of unfavourable wireless channel is the low-cost intelligent reflecting surfaces (IRS) technology, which boosts the received signal's strength and enhances system performance. When direct communications have poor qualities, an IRS intelligently configures the wireless environment to aid the transmissions between the sender and the receiver [4]. It improves the energy efficiency of the signal by radiating all the incident energy in a particular direction towards the destined user. Each of the element of the IRS can be manipulated by changing phase of the incident signals individually. The two different types of OIRS are mirror-based optical IRS and meta-surface-based optical IRS [5]. Mirror-based OIRS mimics a mirror, but in a controllable way, according to the analysis of [4]. Meta-surface-based OIRS are made up of discrete planar arrays of subwavelength unit cells that can change the reflected wave's phase, amplitude, and polarization.

A. Related works

The phased array (PA) and the micro-mirror array (MA) for FSO-based OIRS in a point-to-multipoint FSO communication system are proposed in [6]. According to [6], the optical beam can be converged in the desired direction by mechanically adjusting the orientation of the many micro-mirror modules that make up an MA-based

OIRS. The MA-based OIRS has the potential benefits of low cost and greater reach, allowing it to be used in a variety of communication application scenarios. Similar to RF-based IRS, PA-based OIRS is built from a number of programmable phased modulation units. By varying the phase distribution of the phased modulation units, it is possible to change the beam's form and direction.

In [7], the authors explored the outage probability, average bit error rate (BER), and ergodic capacity utilizing amplify and forward (AF) and DF relays for different water types in which an RF-IRS is utilized in the terrestrial link of a mixed RF-UWOC system. When examining the potential network architecture for an underwater internet of things (IoT), the authors of [8] found that IRS was one of the most promising methods. The authors discussed the advantages of applying IRS in challenging environments (CEs), such as those that are underwater, underground, industrial, or subject to disasters, where signal propagation and communication using conventional signaling systems are easily hampered. Moreover, the authors in [9] use a meta-surface based OIRS and take into account the underwater turbulence, beam attenuation, occlusion or blockage caused by objects, and beam direction errors to evaluate the system performance in terms of BER, channel capacity, and outage probability.

The performance of IRS-assisted UWOC systems when the IRS is positioned in the system's terrestrial connection has received a lot of attention as obvious from the previous literature. The literature, however, is lacking in studies that employ an OIRS that is submerged. Further, a submerged mirror-based OIRS servicing multiple users for UWOC has also not yet been investigated. Consequently, in the proposed work the effectiveness of a submerged mirror-based OIRS with many users in a UWOC system is explored.

B. Motivation and Contributions

To the best of the author's knowledge, the proposed work is first of its kind to propose a novel NLOS technique for underwater communication employing OIRS. An OIRS placed on an autonomous underwater vehicle (AUV) is submerged in water to facilitate communication when direct LOS communication is not possible. In order to maximize the average sum rate and ensure user fairness, the OIRS serves a number of users by allocating a different number of mirror elements to each user.

In light of this, the main contributions of this paper consist of following:

1) This paper proposes a distance-based mirror assignment (DMA) algorithm which takes into account the effects of attenuation and turbulence, for an OIRS assisted UWOC channel.

2) The system is analysed for average sum rate and the user fairness. It can be inferred from the obtained results that DMA not only supports the highest number of users, but also maintains the highest degree of user fairness.

3) We also propose an equal mirror assignment (EMA) algorithm and show that the proposed algorithms perform better in terms of average sum rate and fairness compared to conventional orthogonal multiple access (OMA) and non-orthogonal multiple access (NOMA) techniques.

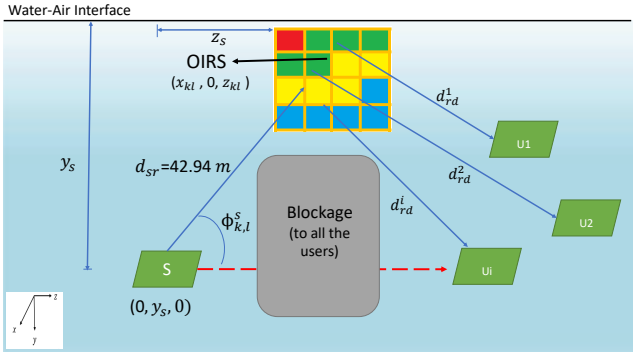

Fig. 1: Schematic for the considered OIRS-aided UWOC system.

II. System Model

Due to the obstructions and changing nature of the water, LOS communication underwater is rarely possible. Thus, NLOS-based communication is the preferred option. The conventional NLOS UWOC design uses the sea surface to make the TIR phenomenon possible, establishing a link between the obstructed transmitter and receiver. Fig. 1 illustrates the system model for an NLOS based UWOC system with OIRS and multiple users.

In this OIRS-aided UWOC system a single source (S) serves as the transmitter for the entire communication system. A planar OIRS is mounted on an AUV that is in direct LOS with the transmitter and multiple users. It is assumed that the communication between the transmitter and receivers (users) occurs via OIRS as the direct LOS communication is blocked. Multiple mirror elements make up the mirror-based OIRS. The OIRS receives the signal from the transmitter and forwards it in the desired user direction by changing the orientation of each OIRS element. A mechanical steering gear individually rotates each OIRS unit's lens-coated surface material [10]. The beam can be focused to a certain location where the size of the target spot is correlated with the size of the mirror unit by adjusting the deflection direction of each mirror unit. The optical signal is not altered in terms of phase, amplitude, or other properties by the OIRS. Further, it is assumed that the AUV with OIRS is situated just below sea surface to ensure that the entire system is submerged. The mobile users are uniformly distributed within a circular area of radius 50 m.

A. Channel Model

In the considered setup, we employ light emitting diodes (LEDs) at the source and a high-sensitivity photodetector (PD), i.e., a silicon photomultiplier (SiPM) at each user. The transmitted signal x from the source having transmitted power of P_t is re-emitted by the OIRS to the intended location. The transmitter is positioned at a depth of y_s from the air-water interface. Thus the received signal at the user is represented as [9],

$$y = G_O h_p h_\alpha x + \Omega, \tag{1}$$

where the OIRS-assisted UWOC system channel gain is denoted by G_O, h_p denotes the attenuation loss, h_α denotes the oceanic turbulence and Ω is the photo current noise, which comprises of shot noise, dark current noise, background noise, and thermal noise. The total noise variance σ_Ω^2 is given by [11],

$$\sigma_\Omega^2 = \sigma_{\rm sh}^2 + \sigma_{\rm d}^2 + \sigma_{\rm b}^2 + \sigma_{\rm th}^2, \tag{2}$$

where $\sigma_{\rm sh}^2$, $\sigma_{\rm d}^2$, $\sigma_{\rm b}^2$ and $\sigma_{\rm th}^2$ denote the variances of the signal shot noise, dark noise, background noise and thermal noise, respectively.

We consider an OIRS with $n_m \times n_m$ mirror elements. Each element has a dimension that is equal to $\ell_m \times w_m$, where ℓ_m and w_m stand for the length and width of a single mirror element, respectively. It is assumed that the OIRS controller is aware of the channel state information (CSI). The channel gain of the reflected signal from each of the OIRS elements in the k^{th} row and ℓ^{th} column is given as [12],

$$G_{{\rm O}_{k,\ell}}(\beta,\Gamma) = \begin{cases} \rho\eta \frac{(m+1)A_{\rm PD}}{2\pi\left(d_{sr}+d_{rd}^i\right)^2}\cos^m\left(\Phi_{k,\ell}^s\right)\cos\left(\psi_{k,\ell}^s\right) \\ \times \cos\left(\Phi_d^{k,\ell}\right)\cos\left(\psi_d^{k,\ell}\right)T(\psi)G(\psi), \\ \qquad\qquad 0 \le \left(\psi_d^{k,\ell}\right) \le (\psi_{FoV}), \\ 0, \qquad\qquad \text{otherwise} \end{cases} \tag{3}$$

where ρ denotes the reflection coefficient of the OIRS element, η is the current-to-light conversion efficiency of the LED, m represents the lambertian order which is given by $m = -\ln(2)/\ln\left(\cos\left(\Phi_{\frac{1}{2}}\right)\right)$, where $\Phi_{\frac{1}{2}}$ is LED semi angle and A_{PD} is the area of the photo diode. $\Phi_{k,\ell}^s$ is the angle of irradiance from the transmitter to OIRS, $\psi_{k,\ell}^s$ is the angle of incidence on the OIRS, $\Phi_d^{k,\ell}$ is the angle of irradiance from the k^{th} row and ℓ^{th} column OIRS element towards the user, and $\psi_d^{k,\ell}$ is the angle of incidence of the reflected signal from OIRS element in the k^{th} row and ℓ^{th} column. The gains of the optical filter and non-imaging concentrator are $T(\psi)$ and $G(\psi)$, respectively, and the field of view (FoV) of the PD is (ψ_{FoV}). The concentrator's gain can be expressed as $G(\psi) = \mu_w^2/\sin^2\psi_{\rm FoV}, 0 \le \psi \le \psi_{\rm FoV}$, where μ_w is the refractive index. The cosine of the angle of irradiance (which is specified by the yaw and roll angles of the mirror array) can be expressed as [13],

$$\cos\left(\Phi_d^{k,\ell}\right) = \frac{(x_{k,\ell}-x_d)}{d_{rd}}\sin(\beta)\cos(\Gamma) + \frac{(y_{k,\ell}-y_d)}{d_{rd}} \times \cos(\beta)\cos(\Gamma) + \frac{(z_{k,\ell}-z_d)}{d_{rd}}\sin(\Gamma),$$

where $(x_{k,\ell}, y_{k,\ell}, z_{k,\ell})$ and (x_d, y_d, z_d) denote the position vectors specifying the locations of the OIRS and the receiver, respectively.

The mirror orientation is obtained by finding a unit vector normal to its surface, $\widehat{\mathbf{N}}_{i,j}$ which can be expressed as [14]

$$\widehat{\mathbf{N}}_{k,\ell} = \frac{\widehat{\mathbf{R_k}_{,\ell}\mathbf{S}} + \widehat{\mathbf{R_k}_{,\ell}\mathbf{D}}}{\sqrt{2 + 2\widehat{\mathbf{R_k}_{,\ell}\mathbf{S}}^T\widehat{\mathbf{R_k}_{,\ell}\mathbf{D}}}}, \tag{4}$$

where the $\widehat{\mathbf{SR}}_{k,\ell}$ represents the corresponding incidence direction and $\widehat{\mathbf{R}_{k,\ell}\mathbf{D}}$ represents the reflection direction. Moreover, $\mathbf{S}, \mathbf{R}_{k,\ell}$ and $\mathbf{D}$ stand for the source coordinates of the source's centre, the centroid coordinates of the mirror in k^{th} row and ℓ^{th} column, respectively, and the destination (user) coordinates. The vectors $\mathbf{S}$, $\mathbf{R}_{k,l}$ and $\mathbf{D}$ are given as

$$\text{S=}\begin{bmatrix} -\left(x_s + \frac{w_m}{2} + (\ell-1)w_m\right) \\ y_s \\ -\left(z_s + \frac{\ell_m}{2} + (k-1)\ell_m\right) \end{bmatrix},$$

$$\text{R}_{k,\ell} = \begin{bmatrix} \left(x_s + \frac{w_m}{2} + (\ell-1)w_m\right) \\ 0 \\ \left(z_s + \frac{\ell_m}{2} + (k-1)\ell_m\right) \end{bmatrix},$$

$$\mathbf{D} = \begin{bmatrix} x_d - \left(x_s + \frac{w_m}{2} + (\ell-1)w_m\right) \\ y_d \\ z_d - \left(z_s + \frac{\ell_m}{2} + (k-1)\ell_m\right) \end{bmatrix}.$$

Furthermore, the rotation angles can be computed using the obtained normal vector $\widehat{\rm N}_{k,\ell}$, as

$$\beta_{k,\ell} = \sin^{-1}\left(\widehat{\rm N}_{k,\ell}^{\rm T}\boldsymbol{e}_3\right) \tag{5}$$

and

$$\Gamma_{k,\ell} = \sin^{-1}\left(\widehat{\rm N}_{k,\ell}^{\rm T}\boldsymbol{e}_1/\cos\left(\beta_{k,\ell}\right)\right) \tag{6}$$

where $\mathbf{e}_c$ $(c \in \{1,2,3\})$ represents the c^{th} column of a 3×3 identity matrix,

The attenuation loss (h_p) in (1) is modelled using the well-known Beer-Lambert law as [3],

$$h_p = e^{-c(\lambda)(d_{sr}+d_{rd}^i)}, \tag{7}$$

where d_{sr} is the distance from the source to the centroid of OIRS, d_{rd}^i is the distance from OIRS to the i^{th} user, and $c(\lambda)$ is the wavelength-dependent extinction/attenuation coefficient and is the summation of the absorption coefficient $a(\lambda)$ and scattering coefficient $b(\lambda)$.

The oceanic turbulence (h_α) can be depicted as a mixture of exponential and generalised gamma (EGG) distributions [15],

$$h_\alpha(\alpha) = \omega f(\alpha;\lambda) + (1-\omega)g(\alpha;[a,b,c]), \tag{8}$$

with

$$f(\alpha;\lambda) = \frac{1}{\lambda}\exp\left(-\frac{\alpha}{\lambda}\right)$$

$$g(\alpha;[a,b,c]) = c\frac{\alpha^{ac-1}}{b^{ac}}\frac{\exp\left(-\left(\frac{\alpha}{b}\right)^c\right)}{\Gamma(a)}.$$

where, f and g denote the exponential and generalized Gamma (GG) distributions respectively, ω is the mixture weight or mixture coefficient of the distributions, satisfying $0 < \omega < 1, \lambda$ is the parameter associated with the

exponential distribution, a, b and c are the parameters of the GG distribution, and $\Gamma(\cdot)$ denotes the Gamma function.

The total path loss (DC gain) for a $n_m \times n_m$ square OIRS-assisted underwater channel is given by using (3), (7), and (8) as [13],

$$H_{OIRS} = \sum_{k=1}^{n_m} \sum_{l=1}^{n_m} G_{\mathrm{O}_{k,l}}(\beta, \Gamma) h_p h_\alpha. \tag{9}$$

The above can be approximated as follows, assuming a point light source case where the distance of light transmission is relatively large compared to the size of the light source and the small OIRS dimensions [12],

$$H_{OIRS} \approx n_m^2 G_{\mathrm{O}_{k,\ell}}(\beta, \Gamma) h_p h_\alpha. \tag{10}$$

Therefore, the overall received power can be given as,

$$P_R = \mathcal{R}_e P_t H_{OIRS}, \tag{11}$$

where P_t is the total transmit power, $\mathcal{R}_e$ is the responsivity of SiPM which is given as [11],

$$\mathcal{R}_{\mathrm{e}} = \left(\frac{\Upsilon_{\mathrm{PDE}}}{E_{\mathrm{ph}}} \right) (1 + P_{\mathrm{AP}} + P_{\mathrm{CT}})\, eG. \tag{12}$$

Here, E_{ph} is the photon energy, and e is the electron charge. Moreover, $G, \Upsilon_{\mathrm{PDE}}, P_{\mathrm{AP}}$, and P_{CT}, stand for the SiPM gain, photon detection efficiency, after-pulsing probability, and crosstalk probability, respectively.

III. Performance Analysis

In this section, we derive the average sum rate of the system and fairness index to investigate the proposed OIRS-assisted UWOC system performance.

A. Average sum rate (ASR)

Using $(2), (10)$, and (11) the instantaneous received electrical SNR is obtained as [11]

$$\gamma_i = \frac{\mathcal{R}_{\mathrm{e}}^2 P_t^2 G_o^2 h_P^2 h_\alpha^2}{\sigma_\Omega^2} = \bar{\gamma_i} h_\alpha^2, \tag{13}$$

where $\bar{\gamma_i} = \frac{\mathcal{R}_e^2 P_t^2 G_o^2 h_p^2}{\sigma_\Omega^2}$ is the average electrical SNR. The data rate for the i^{th} user of the UWOC system is defined as, [16]

$$R_i = \log_2(1 + \tau \gamma_i), \tag{14}$$

where $\tau = \frac{e}{2\pi}$ for IM/DD [17].

The average sum rate is then given as

$$ASR = \sum_{i=1}^{N} R_i. \tag{15}$$

B. Fairness index

We used Jain's fairness index to measure user fairness in this work. All users receive the same average rate if the fairness index value is close to 1. If this index falls almost to zero, a small number of users control the average rate [18].

$$J = \frac{\left(\sum_{i=1}^{N} R_i \right)^2}{N \sum_{i=1}^{N} R_i^2}, \tag{16}$$

where, R_i denotes the individual data rate achieved by the i^{th} user and N is the total number of users.

TABLE I: Simulation Parameters

Parameter	Value
Transmit power (P_t) [19]	1 to 60 dBm
Wavelength (λ_a) [3]	532 nm
Refractive index of water (μ_w) [20]	1.33643
Extinction coefficient of pure seawater $c(\lambda)$ [21]	0.056 m^{-1}
Length of OIRS element ℓ_m	8 cm
Width of OIRS element w_m	8 cm
Reflection efficiency of mirror element ρ [22]	0.8
Lambertian order m [22]	2
Depth of Transmitter y_s	40 m
SiPM area A_{PD}	0.0314 m^2
Optical filter gain T [13]	1
SiPM gain G [11]	10^6
SiPM prob. of cross-talk P_{CT} [11]	0.03%
SiPM prob. of after pulsing P_{AP} [11]	0.2%
Speed of light in water C_{water}	$2.25 \times 10^8 m/sec$
Charge on electron e [11]	1.6×10^{-19} C
Photo current noise Ω [23]	$2{\times}10^{-14} W$
Scintillation index σ_I^2 [15]	{0.2178}
EGG distribution parameters corresponding to σ_I^2 of 0.2178 [15]	
$\{\omega\}$	{0.1665}
$\{\lambda\}$	(0.1207}
$\{a\}$	{0.1559}
$\{b\}$	{1.5216}
$\{c\}$	{22.8754}.

IV. Proposed algorithms:

A. Distance based mirror assignment (DMA) algorithm:

According to this algorithm, the mobile user's distance from the OIRS determines how many mirror elements of the OIRS are assigned to that particular user.

Algorithm 1: Distance based mirror assignment (DMA) algorithm

Input: Initialize $i = (1, ..., N)$ set of users uniformly distributed within the circular area of radius 50 m, an OIRS fixed on an AUV consisting of $n_m \times n_m$ mirror elements where each mirror element is of area 8×8 cm^2.
for i=1, 2..., N **do**
1: Calculate distance of OIRS from the source denoted as d_{sr}
2: Calculate user distances from the OIRS represented as d_{rd}^i
3: Calculate and sort total user distance $(d_{sr} + d_{rd}^i)$ in ascending order
4: Add the distances of all the users from the source (Sum_d)
5: Allocate the number of OIRS elements based on total distance as

$$n_m^i = ceil(\frac{(d_{sr} + d_{rd}^i)}{Sum_d} \times n_m^2)$$

6: Calculate the SNR of i^{th} user using (13)
7: Evaluate the data rate of each user according to (14)
8: The ASR is then calculated by using (15)
8: **end for**

B. Equal mirror assignment (EMA) algorithm:

In this algorithm, the number of mirror elements in the OIRS are divided evenly among all mobile users without

taking into account the distance of the user from the OIRS and the results are compared with the DMA scheme.

C. OMA and NOMA schemes

The OMA scheme used in this work is time division multiple access (TDMA) in which all the OIRS elements are allocated to a single user for one time instant.

For OIRS-assisted NOMA scheme, all the users are allocated equal number of OIRS elements and we assume the perfect successive interference cancellation (SIC) and the fixed power allocation.

V. NUMERICAL RESULTS

In this section, we present the numerical results obtained through the proposed algorithms and compare it with the baseline scenario of OMA and NOMA. The OIRS consist of $n_m \times n_m$ mirror elements with a dimension of $\ell_m = 0.08$ m and $w_m = 0.08$ m. The key simulation parameters are summarized in TABLE I. All the presented results have been obtained through Monte Carlo simulations.

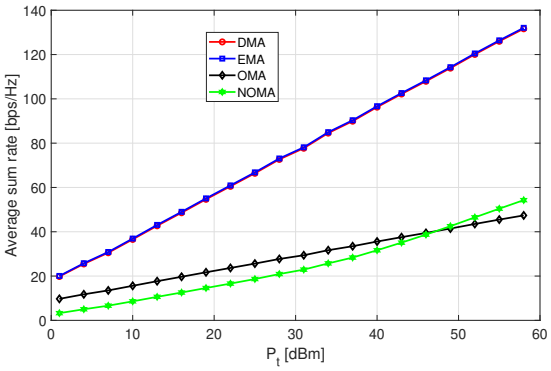

Fig. 2: Average sum rate with respect to transmit power for different assignment schemes, when $N = 3$.

Fig. 2 shows the results for the average sum rate of the four scenarios with regard to the transmit power (P_t) considering 3 users and utilizing EGG distribution for scintillation index (σ_I^2) of 0.2178. The corresponding values of ω, λ, a, b, and c for this scintillation index is given in TABLE I. From Fig. 2, it can be observed that the proposed DMA and EMA based OIRS-assisted UWOC scenarios sum rate is almost same and it outperforms the other schemes. The OIRS elements for small number of users are distributed to all users nearly equally, as is the case with the EMA scheme, which is why the sum rate for the DMA and EMA schemes are the same. Furthermore, it is observed that OMA operates better than NOMA at low P_t because NOMA users experience interference. Yet, NOMA outperforms OMA at high P_t by providing large capacity. As a result, it can be inferred that the proposed algorithms for UWOC systems perform better than the benchmark case in terms of average sum rate.

For $P_t = 10$ dBm, Fig. 3 shows the average sum rate as a function of N. The results demonstrate that DMA is the best scheme for large numbers of users when compared to EMA and OMA since its average sum rate improves significantly as the number of users increases.

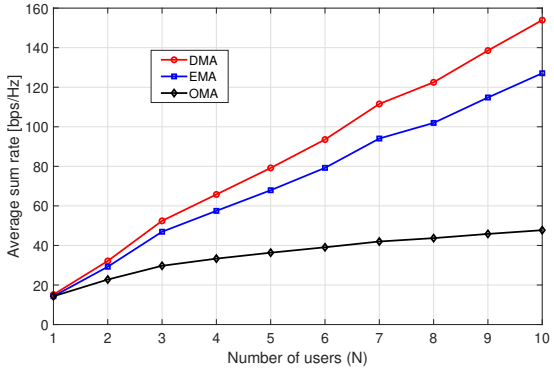

Fig. 3: Average sum rate with respect to number of users for different assignment schemes.

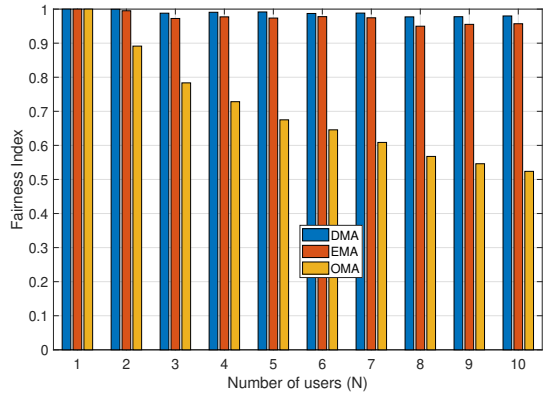

Fig. 4: Fairness index variation with respect to number of users for different assignment schemes.

The fairness index is depicted in Fig. 4 with respect to the number of users. The results show that, for any number of users, the DMA technique is the most fair of the three techniques, followed by the EMA technique. We can also infer that our proposed DMA-based algorithm maintains fairness in addition to achieving the maximum sum rate for a large number of users because the variation in the fairness index of DMA is less than that of the EMA scheme. Additionally, it is determined that as the number of users increases, the fairness of the OMA-based system rapidly declines, making OMA unsuitable for a system that has a large number of users.

Fig. 5 shows the average rate per user with respect to number of users. From the results, it is observed that as the value of N increases, the average rate per user decreases. This drop is due to the fact that when N increases, fewer OIRS elements will be assigned to each user. In OMA, the data rate decreases at much faster rate compared to DMA and EMA schemes. It can be observed that for $N = 10$, the average rate per user in case of OMA reduces to around 6 bps/Hz, whereas it reduces to around 18 bps/Hz for DMA and 15 bps/Hz in case of EMA scheme.

VI. CONCLUSION

An NLOS OIRS-assisted UWOC system is investigated in this paper, and two mirror element assignment tech-

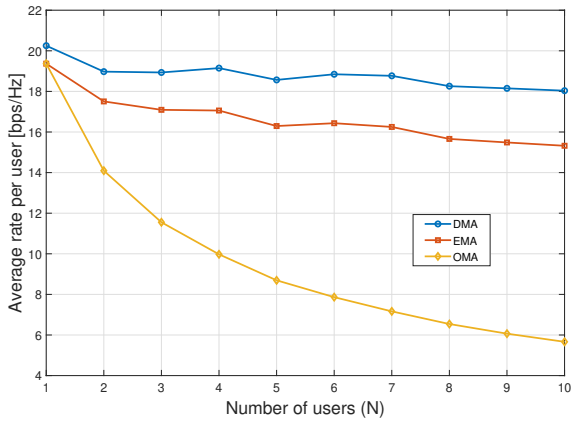

Fig. 5: Average rate per user with respect to number of users for different assignment schemes.

niques (DMA and EMA) are proposed for supporting multiple users. We evaluate the effectiveness of the proposed mirror element assignment techniques taking into account the average sum rate and user fairness. From the results, it is observed that DMA scheme performs better than EMA, OMA, and NOMA schemes in terms of average sum rate as well as user fairness for a large number of users. In future, this work can be extended considering the impact of sea surface slopes (which cause pointing errors) on the overall system performance.

REFERENCES

[1] P. K. Sajmath, R. V. Ravi, and K. A. Majeed, "Underwater wireless optical communication systems: A survey," in *2020 7th International Conference on Smart Structures and Systems (ICSSS)*, 2020, pp. 1–7.

[2] Z. Zeng, S. Fu, H. Zhang, Y. Dong, and J. Cheng, "A survey of underwater optical wireless communications," *IEEE Communications Surveys Tutorials*, vol. 19, no. 1, pp. 204–238, 2017.

[3] H. Kaushal and G. Kaddoum, "Underwater optical wireless communication," *IEEE Access*, vol. 4, pp. 1518–1547, 2016.

[4] V. Jamali, H. Ajam, M. Najafi, B. Schmauss, R. Schober, and H. V. Poor, "Intelligent reflecting surface assisted free-space optical communications," *IEEE Communications Magazine*, vol. 59, no. 10, pp. 57–63, 2021.

[5] S. Aboagye, A. R. Ndjiongue, T. Ngatched, O. Dobre, and H. V. Poor, "RIS-assisted visible light communication systems: A Tutorial," *arXiv preprint arXiv:2204.07198*, 2022.

[6] H. Wang, Z. Zhang, B. Zhu, J. Dang, L. Wu, and Y. Zhang, "Approaches to array-type optical irss: Schemes and comparative analysis," *Journal of Lightwave Technology*, vol. 40, no. 12, pp. 3576–3591, 2022.

[7] S. Li, L. Yang, D. B. d. Costa, M. D. Renzo, and M.-S. Alouini, "On the performance of RIS-assisted dual-hop mixed RF-UWOC systems," *IEEE Transactions on Cognitive Communications and Networking*, vol. 7, no. 2, pp. 340–353, 2021.

[8] S. A. H. Mohsan, A. Mazinani, N. Q. H. Othman, and H. Amjad, "Towards the internet of underwater things: A comprehensive survey," *Earth Science Informatics*, pp. 1–30, 2022.

[9] R. P. Naik and W.-Y. Chung, "Evaluation of reconfigurable intelligent surface-assisted underwater wireless optical communication system," *Journal of Lightwave Technology*, vol. 40, no. 13, pp. 4257–4267, 2022.

[10] V. Jamali, H. Ajam, M. Najafi, B. Schmauss, R. Schober, and H. V. Poor, "Intelligent reflecting surface assisted free-space optical communications," *IEEE Communications Magazine*, vol. 59, no. 10, pp. 57–63, 2021.

[11] I. C. Ijeh, M. A. Khalighi, and S. Hranilovic, "Parameter optimization for an underwater optical wireless vertical link subject to link misalignments," *IEEE Journal of Oceanic Engineering*, vol. 46, no. 4, pp. 1424–1437, 2021.

[12] A. M. Abdelhady, A. K. S. Salem, O. Amin, B. Shihada, and M.-S. Alouini, "Visible light communications via intelligent reflecting surfaces: Metasurfaces vs Mirror arrays," *IEEE Open Journal of the Communications Society*, vol. 2, pp. 1–20, 2021.

[13] S. Aboagye, T. M. N. Ngatched, O. A. Dobre, and A. R. Ndjiongue, "Intelligent reflecting surface-aided indoor visible light communication systems," *IEEE Communications Letters*, vol. 25, no. 12, pp. 3913–3917, 2021.

[14] A. M. Abdelhady, A. K. S. Salem, O. Amin, B. Shihada, and M.-S. Alouini, "Visible light communications via intelligent reflecting surfaces: Metasurfaces vs mirror arrays," *IEEE Open Journal of the Communications Society*, vol. 2, pp. 1–20, 2020.

[15] E. Zedini, H. M. Oubei, A. Kammoun, M. Hamdi, B. S. Ooi, and M.-S. Alouini, "Unified statistical channel model for turbulence-induced fading in underwater wireless optical communication systems," *IEEE Trans. Commun.*, vol. 67, no. 4, pp. 2893–2907, 2019.

[16] H. E. Nistazakis, E. A. Karagianni, A. D. Tsigopoulos, M. E. Fafalios, and G. S. Tombras, "Average capacity of optical wireless communication systems over atmospheric turbulence channels," *Journal of Lightwave Technology*, vol. 27, no. 8, pp. 974–979, 2009.

[17] A. Lapidoth, S. M. Moser, and M. A. Wigger, "On the capacity of free-space optical intensity channels," *IEEE Transactions on Information Theory*, vol. 55, no. 10, pp. 4449–4461, 2009.

[18] R. K. Jain, D.-M. W. Chiu, W. R. Hawe *et al.*, "A quantitative measure of fairness and discrimination," *Eastern Research Laboratory, Digital Equipment Corporation, Hudson, MA*, vol. 21, 1984.

[19] Z. Rahman, N. V. Tailor, S. M. Zafaruddin, and V. K. Chaubey, "Unified performance assessment of optical wireless communication over multi-layer underwater channels," *IEEE Photonics Journal*, vol. 14, no. 5, pp. 1–14, 2022.

[20] S. Arnon and D. Kedar, "Non-line-of-sight underwater optical wireless communication network," *J. Opt. Soc. Amer. A, Opt. Image Sci.*, vol. 26, no. 3, pp. 530–539, 2009.

[21] M. F. Ali, D. N. K. Jayakody, Y. A. Chursin, S. Affes, and S. Dmitry, "Recent advances and future directions on underwater wireless communications," *Archives of Computational Methods in Engineering*, vol. 27, no. 5, pp. 1379–1412, 2020.

[22] L. Zhan, H. Zhao, W. Zhang, and J. Lin, "An optimal scheme for the number of mirrors in vehicular visible light communication via mirror array-based intelligent reflecting surfaces," in *Photonics*, vol. 9, no. 3. MDPI, 2022, p. 129.

[23] M. Elamassie, L. Bariah, M. Uysal, S. Muhaidat, and P. C. Sofotasios, "Capacity analysis of noma-enabled underwater vlc networks," *IEEE Access*, vol. 9, pp. 153 305–153 315, 2021.